Optimal Modifications on Helical Gears for Good Load Distribution and Minimal Wear

Christoph Lohmann, Matthias Walkowiak and Peter Johannes Tenberge

Helical gear teeth are affected by cratering wear — particularly in the regions of low oil film thicknesses, high flank pressures and high sliding speeds. The greatest wear occurs on the pinion — in the area of negative specific sliding. Here the tooth tip radius of the driven gear makes contact with the flank of the driving gear with maximum sliding speed and pressure. In order to understand this phenomenon more precisely, a wear simulation model is presented. Based on an accurate meshing simulation — used to determine the correct path-of-contact by considering tip relief and wear — pressure distribution, sliding speeds and oil film thicknesses across contact lines are calculated. Thus local wear on the teeth of pinion and wheel is calculated via consideration of their roughness. A verification of the model is presented by a comparison of the simulation results with experimental results. Furthermore, a crack criterion to determine critical surface areas regarding micropitting and pitting is presented.

Introduction

Gears can fail due to various damage patterns. Especially in view of the tooth flank fatigue damage such as micropitting or pitting, it is important to be able to recognize and predict the fatigue time. Micropitting starts with fine cracks and small outbreaks on the surface of the flank. It can progressively develop to a cratering wear. Thus, the load capacity of the tooth flank is reduced, additional dynamic loads are arisen and the gear box gets a higher noise level. For a better description of the micropitting area and the wear rate it is necessary to specify the local complex tribological system of the tooth flank.

Experimental results which are presented in Figure 1 have shown that different profile modifications have influence on the micropitting and the wear rate. The commercial calculations accordance to ISO/TR 15144-1 (Ref. 1) does not exactly show the influence of the profile modifications. An optimal modification based on a cubical tip relief with an additional big tooth tip radius causes a smaller micropitting area and wear rate as a modification without a tooth tip radius (Fig. 1). Therefore, the pressure peaks in the first contact area smaller and the risk of the fatigue damage are also smaller.

The meshing engagement of a pair of teeth of a spur gear begins with a first contact of the newly engaging teeth in a contact of the tooth tip radius of the driven gear on the flank of the driving tooth. Meanwhile another pair of teeth is already engaged. In this regard, as the new pair of teeth gets more and more load, the amount of load of the already meshing pair of teeth decreases. In order to take this process accurately into consideration, a precise computation of the path of contact is required. Therewith, the areas of first and last contact starting and leaving the contact at a contact force of zero are considered within a load computation. In case a tip relief and a radius among the flank and head diameter being applied on the teeth, the path of contact differs significantly from the theoretical path of contact of an involute gear without any modifications and sharp edges. The correct path of contact for an improved computation of the load distribution results from a meshing simulation of the actual tooth flanks by taking tooth corrections and wear into consideration. Herewith, it is possible to determine the influence of tip reliefs and tooth tip radii on the load and pressure distribution across the tooth flank, especially in the area of first and last contact, more precise than today.

Based on the local flank pressures, sliding speeds and oil film thicknesses, cratering wear occurs on the teeth of spur gears. Thereby cratering wear occurs especially on the pinion in the area beneath the pitch point where the tooth tip radius of the driven gear gets into contact at a maximum of sliding speed. By taking all the physically relevant parameters into account such a wear mechanism can be computed so that the increase of wear on the tooth flanks can be simulated.
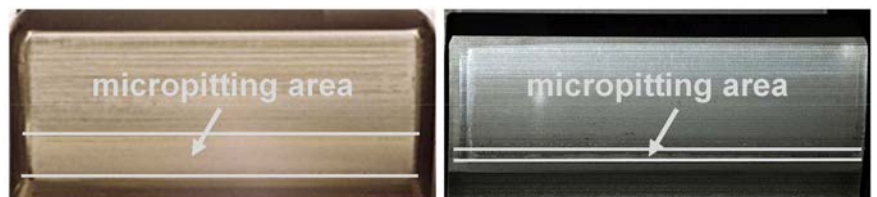
Figure 1   Tooth flanks with micropitting: a) linear tip relief of $c_a = 170\,\mu m$ without an additional tooth tip radius; b) linear tip relief of $c_a = 170\,\mu m$ with an additional tooth tip radius.

Meshing Simulation: Actual Path of Contact

Based on the manufacturing process it is possible to obtain the equations describing the theoretical involute spline of a pinion and a gear wheel within the coordinate system in Figure 2.
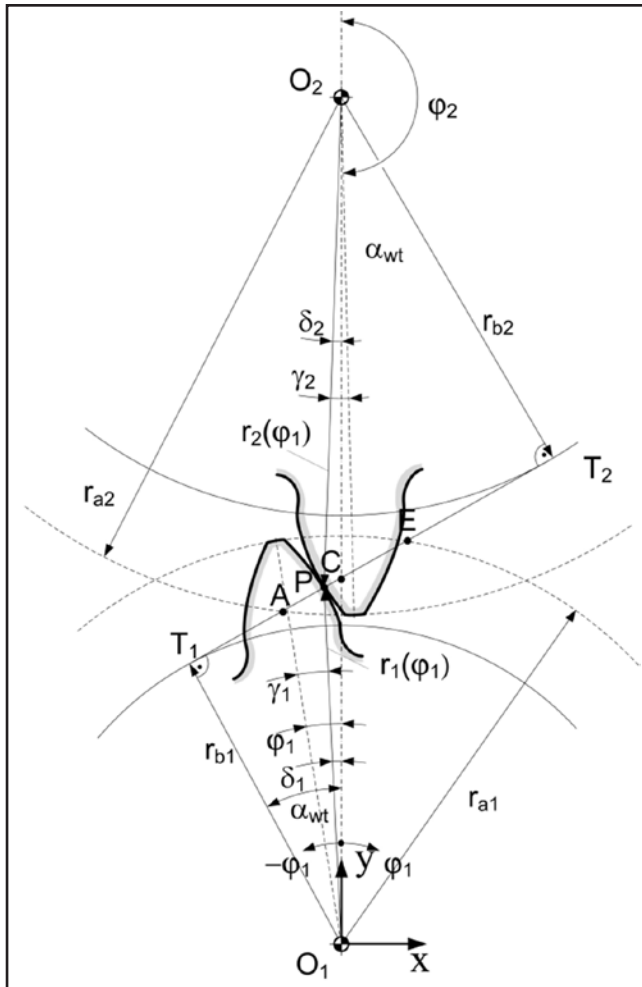
Figure 2   Random position in meshing simulation.

With a meshing simulation the contact points of the pinion and the gear wheel can be found and a line of action can be calculated. The meshing engagement of a pair of teeth of a pinion and a gear wheel begins with a first deflection of the newly-engaging teeth in a contact of the head-edge of the driven tooth on the flank of the driving tooth, while another pair of teeth is already engaged. In that extend as the new pair of teeth gets more and more load, the load on the already meshing tooth pair decreases until it is fully released and tops out.

To calculate this process correctly within a load distribution computation, it requires a precise extension of the line of action up to these areas of first getting in contact at a contact force of zero and leaving the contact at a contact force of again zero. If the teeth have a tip relief and a radius between flank and head-diameter this line of action differs significantly from the theoretical line of action of an involute gear. The correct line of action for an improved load distribution calculation results from a meshing simulation of the actual tooth flanks from the foot-radius beyond the tip radius.

Then it is possible to calculate the influence of different tip reliefs and tip radii on the load distribution on the teeth as well as the pressure distribution.

Therewith, an accurate detection of the point of the first and last contact of gear pairs with profile modifications and cratering wear is possible.

Load Distribution: Local Pressure Distribution

Once the path of contact is derived within a meshing simulation, the load distribution across the contact lines can be computed for a certain number of engagement positions by using contact influence figures (Ref. 5). If the tooth profile has profile corrections or wear, the contact normal forces are not rectified and parallel anymore. This has got to be taken into consideration while formulating the load conservation equation. For a certain amount m of teeth in contact, discretized with a specified number of contact-points n, the discrete load conservation equation arises to Equation 1:

(1)
$$T_{ges} = \sum_{i=1}^{m} \sum_{k=1}^{n} r_{w,i,k} \, F'_{n,i,k}$$

By knowing the parameterized tooth profile, the effective radius r_w arises to Equation 2:

(2)
$$r_{w,i,k}(r_{y,i,k}) = r_{y,i,k} \cos\left(\arctan\left(-\frac{dx_{evo,kor}(r_{y,i,k})}{dy_{evo,kor}(r_{y,i,k})} \right) + \arctan\left(-\frac{x_{evo,kor}(r_{y,i,k})}{y_{evo,kor}(r_{y,i,k})} \right) \right)$$

Because of the fact, that the contact area as well as the load distribution across the contact line and therewith the local Hertzian deformation is unknown, the contact problem has to be solved within an iterative process.

Resulting from the parameterized profile, the local radius of curvature arises to Equation 3, taking profile corrections and wear into consideration. Based on the local radius of curvature:

(3)
$$\rho_{\frac{1}{2}}(r_{y,i,k}) = \left| \frac{[x'_{evo,kor}(r_{y,i,k})^2 + y'_{evo,kor}(r_{y,i,k})^2]^{3/2}}{x'_{evo,kor}(r_{y,i,k}) \, y''_{evo,kor}(r_{y,i,k}) - x''_{evo,kor}(r_{y,i,k}) \, y'_{evo,kor}(r_{y,i,k})} \right|$$

the load distribution resulting from Equation 1 across the path of contact and material constants, the local Hertz contact pressure results from Equation 4:

(4)
$$p_{H,i,k} = \sqrt{ \frac{F_{i,k}}{\Delta l} \; \frac{1}{\rho_{i,k}} \; \frac{1}{\pi\left(\frac{1-v_1^2}{E_1} + \frac{1-v_2^2}{E_2} \right)} }$$

(5)
$$\rho_{i,k} = \frac{\rho_{1,i,k} \rho_{2,i,k}}{\rho_{1,i,k} + \rho_{2,i,k}}$$

Wear-Simulation

Wear on tooth flanks occurs as a result of high sliding speeds, high contact pressure and low oil film thicknesses. Assuming unlimited oil supply and neglecting thermal influences, the local oil film thickness can be computed using Equation 6 with regard to Dowson (Ref. 6), where G is a material coefficient; U a velocity coefficient; W a load coefficient; and ρ the replacement radius of curvature obtained by Equation 5:

(6)
$$h_{min} = 2{,}65 \frac{G^{0,54} U^{0,7}}{W^{0,13}} \rho$$

On the basis of accurate local contact pressures, sliding speeds, specific sliding, local oil film thickness and material hardness, an empirical equation for wear on tooth flanks — such as Equation 7 — can be formulated in accordance with Archard and Holm (Refs. 6, 7, 18):

(7)
$$\frac{dW}{dN} = k_s \cdot k_w \left(\frac{p_H}{2000 MPa} \right)^\alpha \left(\frac{|v_g|}{2 \, m/s} \right)^\beta$$
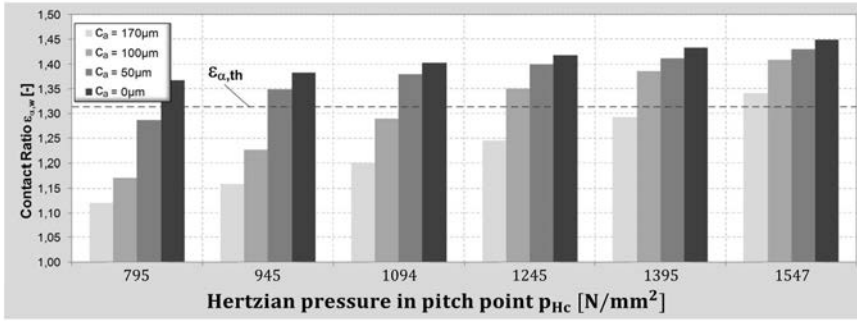
Figure 3   Contact ratio — different profile relief — without wear.
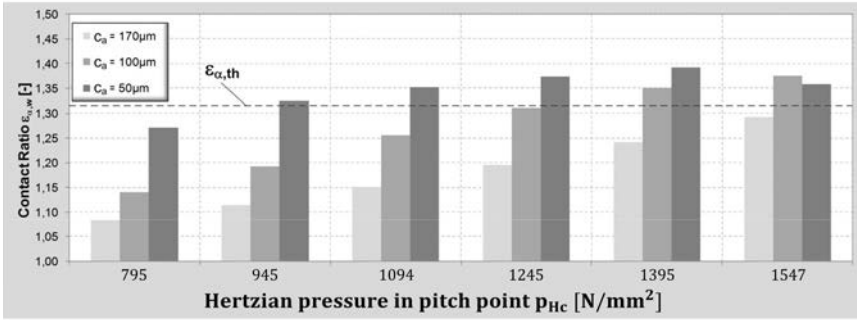

Figure 4   Contact ratio at different profile reliefs — including wear.
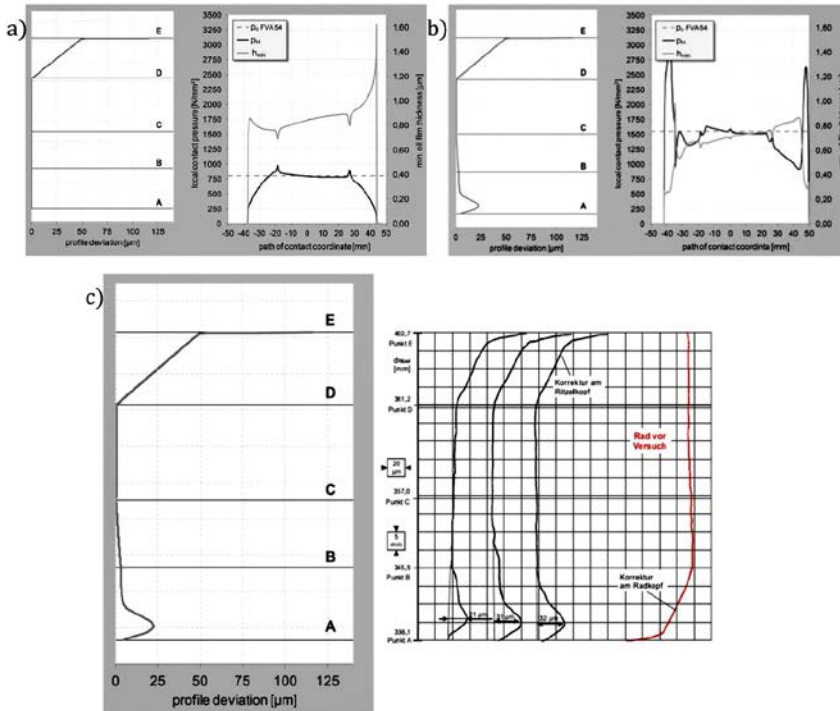
**Figure 5   Contact pressure, min. oil film thickness, profile deviation for tip relief ca = 50 μm: a) before LS5; b) after LS10; c) comparison to test results (Ref. 3).**

$$\left(1 - \left(\frac{0{,}5\mu m}{\sum R_a}\right)^{\kappa} \frac{v_g}{v_\Sigma}\right)^{\chi} \left(\frac{\sum R_a}{h_{min}}\right)^{\gamma} \left(\frac{700HV}{HV_i}\right)^{\delta} \left[\frac{\mu m}{10^6}\right]$$

Herewith the factor k_S considers the chemical characteristics of the lubricant and the factor k_W includes the material properties of the gears. Solving the differential Equation 7 for a specific amount of load cycles dN leads to a certain amount of wear that is transferred onto the tooth profile. Carrying out a new meshing simulation with the newly worn out teeth leads to a changing path of contact in terms of the path of contact of unworn teeth and therewith to an altering load distribution throughout the wear simulation. Thus it is possible to simulate the micropitting test with reference to FVA 54 (Ref. 9). The factor k_S depends on oil type and chemical additive. For each type of lubricant this factor must be governed by an experimental test; it therefore may be used the FZG gear test rig, according to DIN 51354-1.

Comparison to Test Results: Discussion

Subject of the investigation is the influence of the magnitude of tip reliefs on the profile deviation during the micropitting step test in terms of the FVA 54 (Ref. 9) test procedure at an average roughness of $R_a = 0.5\,\mu m$.

Therefore, load steps five to ten are simulated and the computed profile deviation is compared to the profile deviation obtained with the test bench (Ref. 3); gear data used within the experimental tests and the simulation is listed in Table 1.

Taking load into consideration, the effective contact ratio can be computed by solving Equation 1 for a certain number of engagement positions. Figure 3 shows the true contact ratio ε_{aw} for the investigated tip reliefs for the load steps LS5 to LS10 without wear. A higher amount of tip relief results in a lower effective contact ratio within all six load steps.

Table 1	Gear set data		pinion	wheel
Normal module	m_n	[mm]	22	
Nuber of teeth	z	[-]	16	24
Profile shift factor	x	[-]	0,1817	0,1715
Helix angle	β	[°]	0	
Pressure angle	$α_n$	[°]	20	
Operating pressure angle	$α_{wt}$	[°]	22,4	
Center distance	a	[mm]	447,334	
Face width	b	[mm]	105	100
Profile contact ratio	$ε_a$	[-]	1,31	
Average roughness	R_a	μm	0,5	0,5
Speed	n	[1/min]	450	300
Tip diameter	d_a	[mm]	402,69	570,62
Root diameter	d_f	[mm]	304,96	480,55
Oil viskosity	v_{40}	[mm²/s]	220	
Oil type		[-]	mineral oil with A99	

With increasing load, the effective contact ratio increases.

Within the simulation process, wear is computed for a specific amount of load cycles dN using Equation 7 and transferred onto the tooth profile. This leads to an altering circumferential backlash throughout time. In Figure 4 the effective contact ratio ε_{aw} is shown after $2.1 \cdot 10^6$ load cycles for each load step.

For a tip relief of $c_a = 50\,\mu m$, the effective contact ratio increases with the load step till load step LS9. Within load step LS10 the growth of wear due to contact pressure and sliding speeds in the area of first contact causes a decrease in the effective contact ratio. For a tip relief of $c_a = 100\,\mu m$ and $c_a = 170\,\mu m$ the effective contact ratio increases with load, but basically the effective contact ratio is less compared to the simulation without wear.

Figure 5 a) left shows the simulated profile deviation of the pinion before start of load step LS5 with a tip relief of $c_a = 50\,\mu m$. On the right, the course of the contact pressure and oil film thickness vs. path-of-contact coordinate is depicted. In the area of first and last contact the contact pressure declines to zero. At the engagement points B and D the linear tip relief converges into the involute spline — which results into a small local radius of curvature and therefore an increase in the local pressure and a decrease in the local oil film thickness.

Figure 5 b) left shows the simulated profile deviation of the pinion after finishing LS10 with $12.6 \cdot 10^6$ load cycles. In the area of first contact with the highest amount of sliding speeds, the oil film thickness collapses because of aggravating contact conditions due to the occurring wear. Within this area cratering wear occurs on the pinion. A comparison of the simulated wear with the test results in Figure 5 c) shows a very good correlation between the simulation and the experimental results.

Figure 6 a) left shows the simulated profile deviation of the pinion before start of load step LS5 with a tip relief of $c_a = 100\,\mu m$. Comparing Figure 6 a) right to Figure 5 a) right, it can be stated that the effective contact ratio decreases with an increase in the amount of tip relief. The small radius of curvature at the engagement points B and D, where the linear tip relief converges into the involute spline, causes peaks within the course of the local contact pressure, and a collapse in the local oil film thickness.

Figure 6 b) left shows the simulated profile deviation of the pinion after finishing load step LS10. Due to the higher amount of tip relief
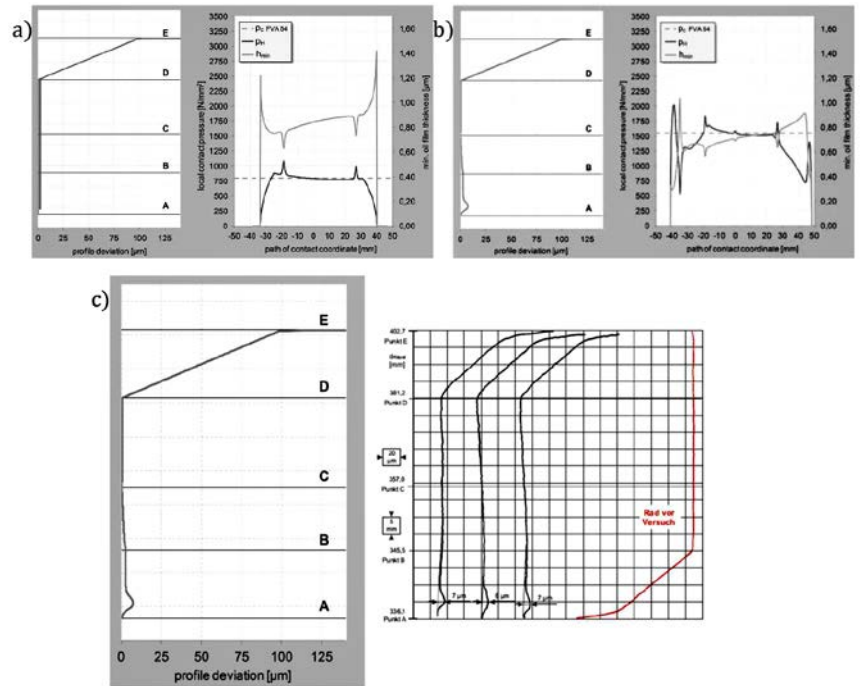
Figure 6 Contact pressure, min. oil film thickness, profile deviation for tip relief ca = 100 μm: a) before LS5; b) after LS10; c) comparison to test results (Ref. 3).
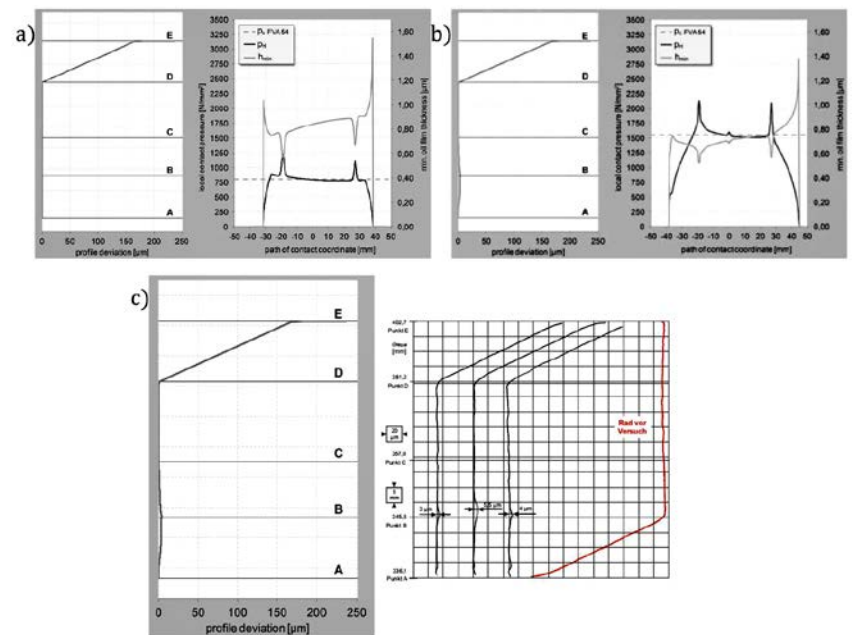
**Figure 7** Contact pressure, min. oil film thickness, profile deviation for tip relief ca = 170 μm: a) before LS5; b) after LS10; c) comparison to test results (Ref. 3).

the magnitude of wear in the area of first contact is less compared to Figure 5 b) left, but cratering wear still occurs.

A comparison of the simulated wear with the test results in Figure 6 c) shows a very good correlation between the simulation and the experimental results.

Figure 7 a) left shows the simulated profile deviation of the pinion before start of LS5 with a tip relief of $c_a = 170\,\mu m$.

Again, the small radius of curvature at the engagement points B and D causes peaks within the course of the local contact pressure and a collapse in the local oil film thickness.

Due to the applied tip relief of $c_a = 170\,\mu m$, the point of first contact occurs subsequently and the effective contact ratio declines in comparison to variants with less tip relief. After finishing load step LS10, the maximum local contact pressure and the minimum oil film thickness occur at the engagement point
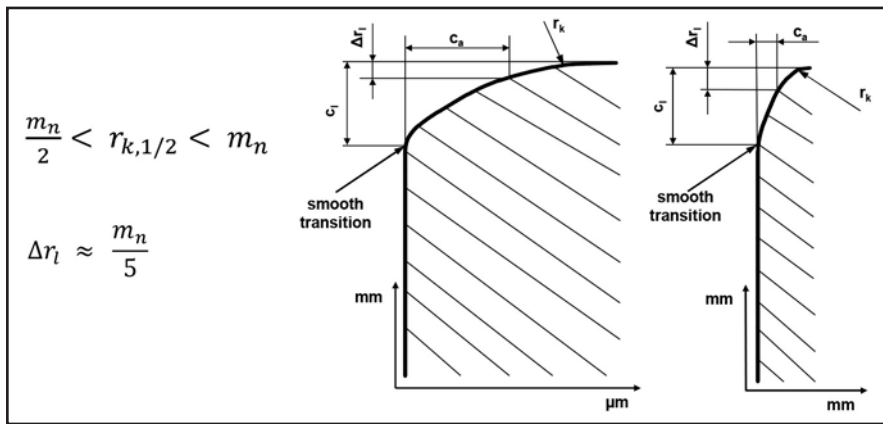
Figure 8   Optimal profile modification.

B. Therefore the location of maximum wear shifts from the point of first contact to the engagement point B.

A comparison of the simulated wear with the test results in Figure 7 c) shows a very good correlation between the simulation and the experimental results.

With an optimal profile modification pressure peaks could be avoided. An optimal profile modification consists of a smooth transition without sharp edges between involute profile and profile modifications and an additional tooth tip radius for smooth first contact. Figure 8 shows an optimal profile modification.

Crack Criterion

Micropitting or grey staining is a fatigue failure on tooth flanks, which is mainly influenced by local contact pressures, sliding speeds and lubrication conditions. It starts with micro-cracks on the surface of the flanks. Herewith, micropitting acts like a profile deviation on flanks in the area of negative specific sliding. Within this area, the tooth tip radius of the driven gear gets into contact with the dedendum of the driving gear.

Based on the fatigue phenomenon, the fatigue processes in the tooth flank contact can be described in detail. Two stages are distinguished here: Stage 1, the crack initiation, and Stage 2, the crack growth. Cracks occur where specific crack criteria are satisfied. Because of periodic stress in the tooth contact, the cracks can grow in their crack tips.

Cracks occur because of the stress superposition from the Hertzian contact stresses and near-surface shear stresses. The

near-surface shear stresses result from the sliding speed on the tooth flanks and the friction coefficient between the contact bodies. Boundary and hydrodynamic friction are separated here.

Containing the local flank pressures, the local rolling and sliding speeds, the local film thicknesses and further parameters from the meshing simulation, an empirical criterion for the initial cracking is presented for the contact of two tooth flanks. It is based on the Ruiz-Chen criterion (Ref. 4). It states that if two bodies are under dynamic load in contact, the product of the sliding path and shear stress is responsible for the first crack; this product can be regarded as friction energy. But the tangential tensile stress in the direction of the slip is also important for the crack beginning and for the crack characteristics. This is transferred to a gear and for the description of the tribological system the factor is upgraded with the relative lubricant film thickness. Equation 8 shows a first approach for such a crack criterion:

(8)

$$R = \frac{1}{750}\left(\frac{p_H}{[\text{MPa}]}\right)^\alpha \left(\frac{s_g}{[\text{mm}]}\right)^\beta e^{-(\gamma\lambda)}\left(1-\frac{v_g}{v_\Sigma}\right)$$

The crack criterion implies that in the case of two contacting tooth flanks under load, the product of an equivalent stress σ^α_{vG}, sliding path S^β_g and the relative film thickness λ in the area of negative specific sliding, are responsible for the crack initiation. Thus an equivalent stress needs to be defined; for example, by means of the stresses of the Hertzian contact and the near-surface tangential stresses. The equivalent stress must have a maximum in an angle, which is determined by experimental results of micropitting.

The sliding path between two contacting tooth flanks is given by Equation 9 from the product of the sliding speed v_g and the time Δt. The sliding path is limited by the Hertzian contact width $2b_H$. During the time Δt the flank area $2b_H$ is in contact with the opposite flank by the rolling speed v_t.

(9)

$$s_g = \Delta t\, v_g = \frac{2b_H}{v_{t,\frac{1}{2}}} v_g$$

The relative lubricant film thickness λ is the ratio of the minimum lubricant film thickness and the surface roughness of the tooth flanks. Reference 3 shows that the reduction of the relative film thickness, increased by growing roughness, leads to micropitting. Therefore the Ruiz-Chen criterion is extended by this factor.
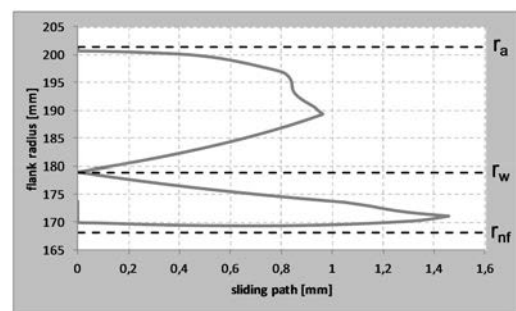

Figure 9   Sliding path over the flank area of the driven gear $m_n = 22\,mm$.

$$\lambda = \frac{h_{min}}{\frac{1}{n}\sum_{i=1}^{n} Ra_i} \qquad (10)$$
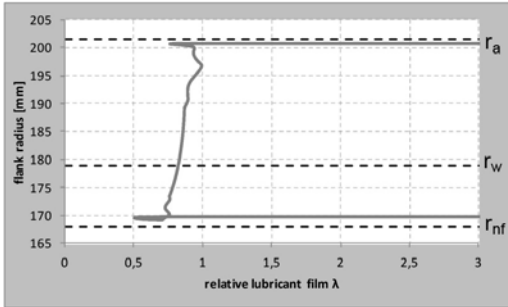
Figure 10   Relative oil film thickness versus the flank area of the driven gear mn = 22 mm

Micropitting preferentially occurs in the area of negative specific sliding, where the material is drifted due to the opposite direction of rolling and sliding speed. In this flank area the risk of cracks is significantly higher. This characteristic is included in Equation 8, with the factor $\left(1 - \frac{v_g}{v_\Sigma}\right)$.

By means of such an empirical crack criterion, Equation 8, which is taking into account the stress conditions, the sliding speeds of the surface, and the lubrication condition, the critical surface areas regarding micropitting can be detected (Fig. 10). The exponents α, β and γ of Equation 8 must be determined with experimental results. Furthermore, a critical value R_{crit} must be defined, which indicates an increased risk of micropitting if the critical value is exceeded. The crack criterion is normalized to $R_{crit} = 1$. The criterion was validated by using the results of experimental results of Reference 3, (Fig. 10). The crack criterion agreed very well with the experimental results.
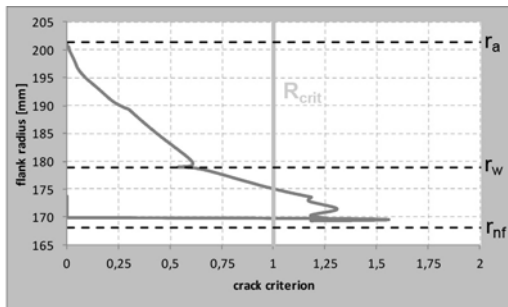

Figure 11   Crack criterion indicating the flank region with higher risk of cracking.

Summary

The presented algorithm combines a meshing simulation based on the tooth profile, taking corrections and wear into consideration, with a load algorithm including shaft and bearing deformation. It therefore follows that an accurate detection of the point of first and last contact is possible.

Based on the precise computation of the contact pressure, sliding speeds, and oil film thicknesses, a wear simulation for load and rotation spectra is presented. A comparison of the simulation with test results demonstrates a good accordance and confirms the approach. Therefore, an optimal profile modification with a quadratic or cubical tip relief and a tooth tip radius can calculate against micropitting or pitting. Furthermore, a crack criterion to determine the locations of micropitting is presented. ⚙

References

1. ISO/TR 15144-1. Calculation of Micropitting Load Capacity of Cylindrical Spur and Helical Gears — Part 1: Introduction and Basic Principles, 2010.
2. Linke, H. Stirnradverzahnung – Berechnung Werkstoffe Fertigung, Carl Hanser Verlag Munchen Wien, 1996 Gottingen.
3. Lutzig, G. Gro.getriebe-Graufleckigkeit: Einfluss von Flankenmodifikationen und Oberflachenrauheit, Dissertation, Ruhr-Universitat Bochum, Bochum, 2006.
4. Ruiz, C. and K.C. Chen. "Life Assessment of Dovetail Joints Between Blades and Discs in Aero Engines," *Fatigue of Engineering and Structures*, Institute of Mechanical Engineers, London, 1986, 187-194.
5. Kunert, J. "Experimentell Gestutzte Untersuchung zum Verformungs-und Spannungsverhalten an au.Enverzahnten Stirnradern fur eine Verbesserte Beanspruchungsanalyse," Dissertation, Technische Universitat Dresden, August 1998.
6. Wisniewski, M. "Elastohydrodynamische Schmierung, Grundlagen und Anwendungen, Handbuch der Tribologie und Schmierungstechnik," Band 9, Expert-Verlag, Renningen-Malmsheim, 2000.
7. Suh, N. P. "The Delamination Theory of Wear," *Wear* 25, 1973.
8. Kragelskij, I.V., N. Dobyčin and V. "Kombalov. Sergeevič: Grundlagen der Berechnung von Reibung und Verschleifs," Munchen, Wien: Hanser, 1983.
9. FVA - Informationsblatt Nr. 54/I – IV. "Testverfahren zur Untersuchung des Schmierstoffeinflusses auf die Entstehung von Grauflecken bei Zahnradern," Frankfurt, 1993
10. Walkowiak, M. "Ortliche Belastungen und Verschleifsiulation in den Zahneingriffen Profilkorrigierter," Gerad-und Schragverzahnter Stirnradgetriebe Zwischen Einfederungsbeginn und Ausfederungsende, Dissertation, Ruhr-Universitat Bochum, Bochum 2013.

Christoph Lohmann studied mechanical engineering at the University of Applied Sciences of the Lower Rhine in Krefeld and at the Ruhr University Bochum, graduating as a cooperative engineer-in-training at Bayer AG. He concluded his studies in 2012 with his master's thesis — "Simulation of System Dynamics of Heavy Drivetrains with Multi-Body Simulation" — at SEW-Eurodrive GmbH & Co KG in Bruchsal. In 2012 he started as a research assistant at the Chair of Industrial and Automotive Drivetrains of Prof. P. Tenberge. Lohmann's fields of research are tooth contact analysis, tooth profile modifications, fatigue failure and tribological stresses.

Prof. Dr.-Ing. Peter Johannes Tenberge since 2012 is Chair of industrial and automotive drivetrains at Ruhr-University Bochum. He has previously served (1994-2012) as professor for machine elements at Chemnitz University; (1992-1994) general manager for development and sales of INA Motorenelemente Schaeffler KG; (1989-1992) head of R&D of INA Wälzlager Schaeffler KG; and (1986-1989) as a project engineer at Zahnradfabrik Friedrichshafen AG. Tenberge has, in his career thus far, proposed for automotive applications several transmission concepts for AT, DCT, CVT and Hybrids, and in 2012 was awarded the SAE/Timken Howard Simpson Automotive Transmission and Driveline Innovation Award. He also keeps busy working on various industrial applications in which he works on design, development and simulation tools for a more precise and quicker layout of transfer gears, worms gear, bevel gears and planetary gears. Tenberge is also the holder or co-holder of more than 200 national and international patent applications.

Dr.-Ing. Matthias Walkowiak has since 2013 worked as a calculation and development engineer at SEW-Eurodrive GmbH & Co KG in Bruchsal. Upon receipt of his engineering degree he began his career at the chair of Machine Elements, Gears and Motor Vehicles of Prof. W. Predki at the Ruhr University Bochum as a research assistant. He completed his PhD successfully in 2013 with the doctoral thesis, "Local Loads and Wear Simulation of Tooth Meshing on Spur and Helical Gears with Profile Modifications Between the Beginning and the Ending of the Deflection," at the chair of Industrial and Automotive Drivetrains of Prof. P. Tenberge.